A Comprehensive Study of Carbon Nanotube Based Transistors: The Effects of Geometrical, Interface Barrier, and Scattering Parameters

M. Pourfath, H. Kosina, and S. Selberherr
Gußhausstraße 27–29/E360, 1040 Wien, Austria
Phone: +43-1-58801/36031, Fax: +43-1-58801/36099
{pourfath|kosina|selberherr}@iue.tuwien.ac.at

Abstract

The performance of carbon nanotube field-effect transistors has been studied based on the non-equilibrium Green's function formalism. The effects of elastic and inelastic scattering and the impact of parameters, such as electron-phonon coupling strength and phonon energy, on the device performance are analyzed. The effect of scaling of the source-gate spacer, drain-gate spacer, and gate length is studied. The results for devices with different barrier heights at the metal-CNT interface are discussed.

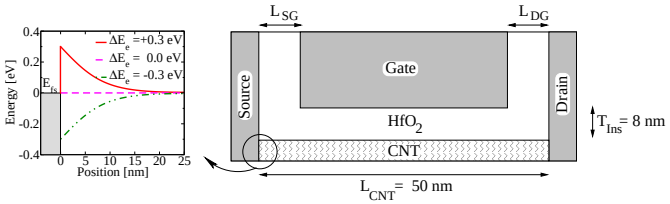

Fig. 1. Cross section of the device and the band-edge profile at the source sided metal-CNT interface. Depending on the work function difference between metal and CNT positive, zero, and negative barrier heights for electrons or holes can be achieved. In this work we assume electrons as majority carriers. Due to the symmetric band structure, the conclusions also hold for holes.

Introduction

Carbon nanotube (CNT) based transistors have been studied in recent years as potential alternatives to CMOS devices because of their capability of near ballistic transport [1]. Depending on the work function difference between the metal contact and the CNT, carriers at the metal-CNT interface encounter different barrier heights (the definition of the barrier height is seen in Fig. 1). Fabrication of devices with positive (Schottky type) [2] and zero (Ohmic) [1] barrier heights for holes have been reported. Here electrons are considered to be majority carriers. Since the dispersion relations for electrons and holes are symmetric, our discussions are valid for holes as well. The gate voltage controls the current by modulating the transmission coefficient of carriers through the device [1].

In this work the non-equilibrium Green's function (NEGF) formalism is used to perform a comprehensive numerical study of CNT based transistors. Electron-phonon interaction parameters depend on the chirality and the diameter of the nanotube. For the first time, the device response is studied for a wide range of electron-phonon interaction parameters. Extending previous work [3, 4] the effects of scaling of source-gate spacer ($L_{\rm SG}$) and drain-gate spacer ($L_{\rm DG}$) (Fig. 1) on the device characteristics are investigated in detail. The results indicate that these effects can be very different from conventional MOSFETs. The effect of geometrical parameters on the device characteristics strongly depends on the barrier height at the metal-CNT interface for majority carriers. As a result, a careful selection of geometrical parameters leads to considerable improvement of device performance.

Approach

The NEGF formalism has been employed [7]. The transport equations are solved on the surface of the CNT. We assume bias conditions in which the first sub-band contributes mostly to the total current. In the mode-space approach the transport equations for each sub-band can be written as [8]:

$$G^{\rm R,A}(E) = [EI - H(E) - \Sigma^{\rm R,A}(E)]^{-1} \tag{1}$$

$$G^{<,>}(E) = G^{\rm R}(E)\Sigma^{<,>}(E)G^{\rm A}(E) \tag{2}$$

We consider the self-energies due to contacts and electron-phonon interaction, $\Sigma = \Sigma_{\rm s} + \Sigma_{\rm d} + \Sigma_{\rm e-ph}$. The self-energy due to the coupling of the device to the source and drain contacts is only non-zero at the boundaries. The self-energy due to electron-phonon interaction comprises the contributions of elastic and inelastic scattering mechanisms, $\Sigma_{\rm e-ph} = \Sigma_{\rm el} + \Sigma_{\rm inel}$, where the terms are given by:

$$\Sigma_{\rm el}^{<,>}(E) = D_{\rm el}G^{<,>}(E) \tag{3}$$

$$\begin{aligned}\Sigma_{\rm inel}^{<}(E) = &\sum_{\nu} D_{\rm inel}^{\nu} \\ &\times[(n_B(\hbar\omega_\nu)+1)G^{<}(E+\hbar\omega_\nu) \\ &+n_B(\hbar\omega_\nu)G^{<}(E-\hbar\omega_\nu)]\end{aligned} \tag{4}$$

where D is electron-phonon coupling coefficient, $\hbar\omega$ is the phonon energy, and ν is the phonon mode. $\Sigma_{\rm inel}^{>}$ is calculated similarly to (4) [8]. Assuming thermal equilibrium for phonons, their occupation number is given by the Bose-Einstein distribution function.

1-4244-0438-X/06/$20.00 ©2006 IEEE

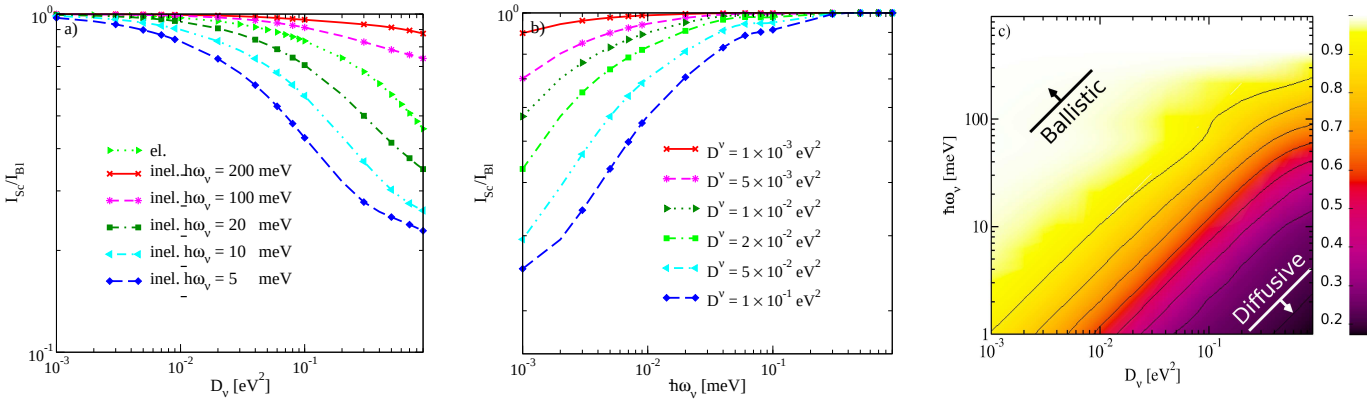

Fig. 2. a) The ballisticity versus the strength of electron-phonon coupling for a CNT of 50 nm length. The ballisticity is defined as the ratio of the on-current in the presence of electron-phonon interaction to the current in the ballistic case $I_{\rm Sc}/I_{\rm Bl}$. b) The ballisticity versus the phonon energy. c) Ballisticity versus both the strength of electron-phonon coupling and phonon energy.

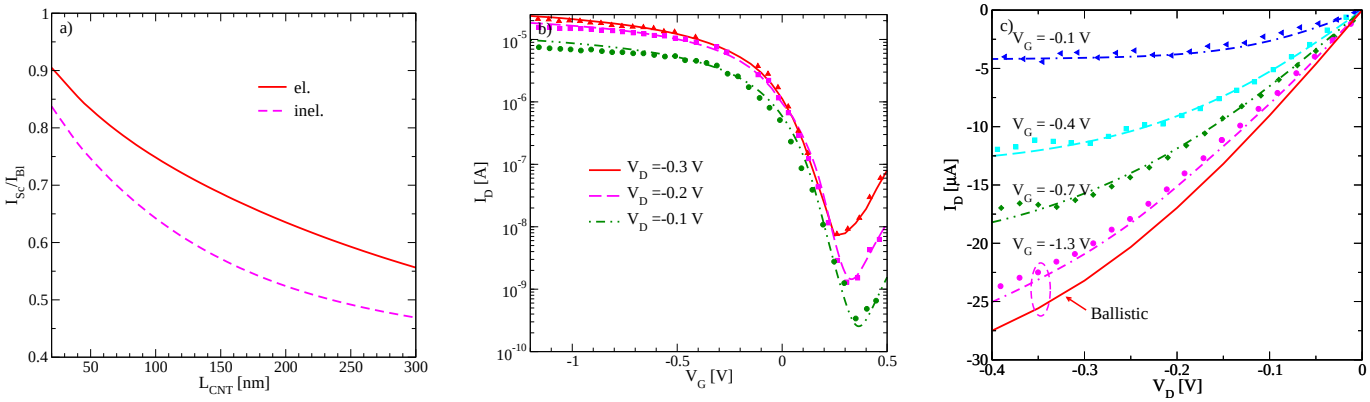

Fig. 3. a) Ballisticity versus CNT length. The following parameters were used for elastic scattering $D_{\rm el} = 10^{-1}$ eV^2 and for inelastic scattering $D_{\rm inel} = 10^{-1}$ eV^2 and $\hbar\omega_{\rm inel} = 25$ meV. Comparison of the simulation results and experimental data for the b) transfer and c) output characteristics. Lines show the simulation results and symbols show experimental data. The result for $V_{\rm G} = -1.3$ V is compared with the ballistic limit. Elastic scattering occur due to acoustic phonons (AP), and inelastic scattering due to zone boundary (ZB), optical (OP), and radial breathing (RBM) phonon modes. The electron-phonon interaction parameters were selected as follows: $D_{\rm AP} \approx 10^{-4}$ eV^2, $D_{\rm ZB} \approx 10^{-4}$ and 50×10^{-3} eV^2, $\hbar\omega_{\rm ZB} \approx 160$ and 180 meV, $D_{\rm OP} \approx 40 \times 10^{-3}$ eV^2, $\hbar\omega_{\rm OP} \approx 200$ meV, $D_{\rm RBM} \approx 10^{-3}$ eV^2, $\hbar\omega_{\rm RBM} \approx 30$ meV [5, 6]. High energy phonons, such as OP and ZB phonon modes, degrade the performance only weakly, whereas the RBM phonon mode can have a detrimental effect. However, due to weak electron-phonon coupling, the RBM mode has a negligible effect even at room temperature.

The imaginary and real parts of the self-energy broadens and shifts the density of states, respectively. Here, the imaginary part of the self-energy, which adds dissipation to the Hamiltonian, is considered and the real part is neglected [9].

$$\Im m[\Sigma^{\rm R}(E)] = \frac{1}{2i}[\Sigma^{>} - \Sigma^{<}] \qquad (5)$$

The transport equations and the Poisson equation are coupled self-consistently.

The Effect of Scattering Parameters

The scattering parameters, D_ν and $\hbar\omega_\nu$, depend on the chirality and the diameter of the CNT. The calculation of these parameters is presented in [5]. Due to many possible configurations of the CNT lattice, the device response is studied for a wide range of electron-phonon interaction parameters. With increasing D_ν the self-energy increases, which adds dissipation to the Hamiltonian, and consequently the total current decreases. Fig. 2-a shows the ballisticity as a function of D_ν. Elastic scattering conserves the energy of carriers, but the current decreases due to elastic back-scattering. On the other hand, with inelastic scattering the energy of carriers is not conserved. Carriers acquiring enough kinetic energy can emit phonons and scatter into lower energy states. With the increase of $\hbar\omega_\nu$ the current is less reduced, since scattered carriers lose more kinetic energy and the probability for back-scattering decreases, see Fig. 2-b. For a better comparison, Fig. 2-c shows regions of ballistic and diffusive transport for inelastic scattering. These results are for a device of 50 nm length. Fig. 3-a shows that the ballisticity is inversely proportional to the CNT length. Fig. 3-b and Fig. 3-c show excellent agreement between simulation results and experimental data [10]. The results indicate that devices with a channel length of less than several hundred nanometers can operate close to the ballistic limit.

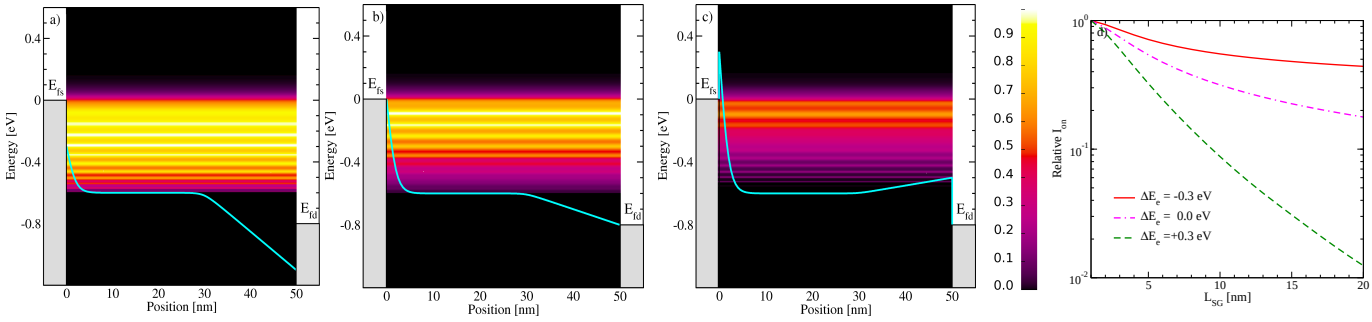

Fig. 4. The normalized spectrum of current based on ballistic transport for a device with a) negative, b) zero, and c) positive barrier height. $V_{\rm G} = 0.6$ V and $V_{\rm D} = 0.8$ V. d) The relative variation of the on-current versus the source-gate spacer.

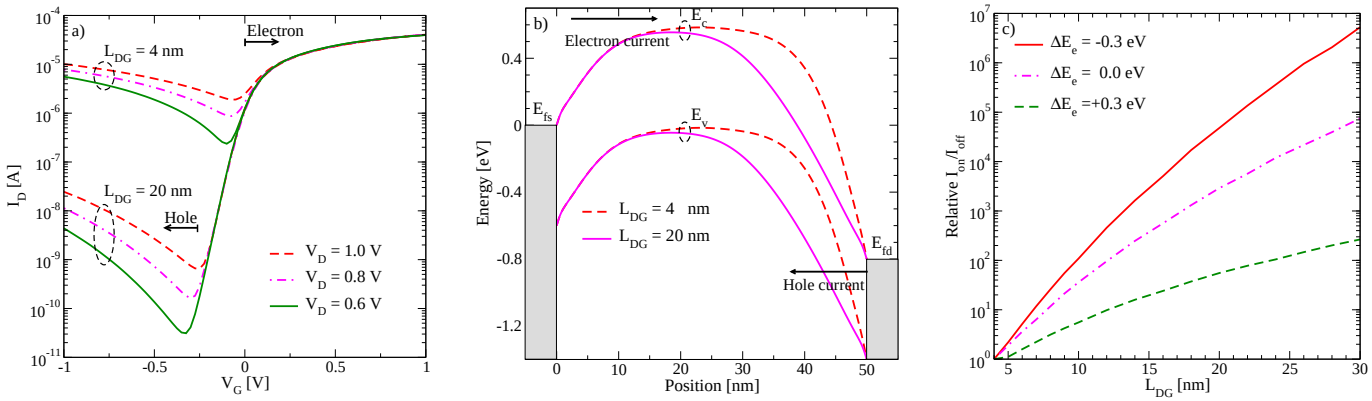

Fig. 5. a) Transfer characteristics for the device with zero barrier height. At the minimum current points electrons and holes have the same contribution to the total current, whereas in other regions either the electron or hole contribution will dominate. b) Comparison of the band-edge profile for devices with $L_{\rm DG} = 4$ nm and $L_{\rm DG} = 20$ nm. $V_{\rm G} = 0.6$ V and $V_{\rm D} = 0.8$ V. c) The ratio of the $I_{\rm on}/I_{\rm off}$ versus $L_{\rm DG}$.

The Effect of Geometrical Parameters

In this section the effect of source-gate and drain-gate spacer lengths on the device response is investigated. Both the tunneling current and thermionic emission current contribute to the total current, see Fig. 4. Electrons with energies lower than the barrier height have to tunnel through the source-sided metal-CNT interface barrier to reach the channel, while electrons with higher energies are injected by thermionic emission. Fig. 4 shows that at high gate bias even for devices with zero or negative barrier height the tunneling current contributes considerably to the total current. Since the tunneling probability decreases exponentially with the barrier width, the tunneling current decreases with increasing $L_{\rm SG}$. Fig. 4-d shows the on-current versus $L_{\rm SG}$. Since the contribution of tunneling current decreases with decreasing barrier height, the on-current is less sensitive to $L_{\rm SG}$ in devices with negative barrier heights.

The transfer characteristics at different drain biases are shown in Fig. 5-a. In the off-regime the drain current starts to increase due to ambipolar conduction. By increasing the drain bias this phenomenon becomes more apparent [10, 11]. Fig. 5-b shows that if the drain voltage becomes higher than the gate voltage, the barrier thickness for holes at the drain contact is reduced and the tunneling current of holes increases. By increasing $L_{\rm DG}$ the band edge profile near the drain contact is less affected by the gate voltage. As a result, the parasitic tunneling current is suppressed. Fig. 5-c compares the increase of the $I_{\rm on}/I_{\rm off}$ ratio versus $L_{\rm d}$. When increasing $L_{\rm d}$, the off-current decreases, while the on-current remains nearly unchanged, such that the $I_{\rm on}/I_{\rm off}$ ratio increases. In devices with negative barrier height more improvement is achieved, since in such devices the off-current is mostly due to parasitic tunneling rather than thermionic emission.

Fig. 6 shows the effect of $L_{\rm DG}$ on the output characteristics for devices with different barrier height. In the device with positive barrier height the current at low drain biases decreases as $L_{\rm DG}$ increases. This can be well understood by considering Fig. 4-c. In a device with positive barrier height electrons at the drain-sided metal-CNT interface have to tunnel through the barrier to reach the drain contact. Similar to what we discussed for $L_{\rm SG}$, with increasing $L_{\rm DG}$ the thickness of the barrier increases and the drain current is reduced. If the drain voltage becomes higher than the gate voltage, most of the electrons can reach the drain contact by thermionic emission. In devices with negative and zero

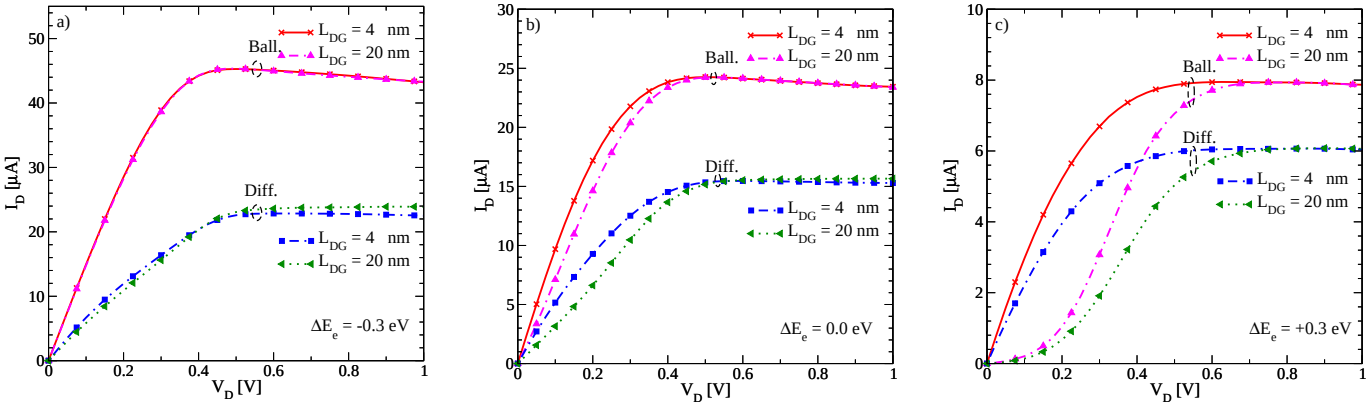

Fig. 6. The effect of L_{DG} on the output characteristics for the device with a) negative, b) zero, and c) positive barrier height. For all simulation results $V_{\mathrm{G}} = 0.5$ V. In all cases the results for both ballistic and diffusive transport are shown. The results indicated that the ungated region does not increase the channel resistance. The decrease of the current at low biases for a device with positive barrier height is due to the barrier formed at the drain-sided metal-CNT interface. For diffusive transport we assumed strong electron-phonon coupling and low energy phonos. The following parameters were used for inelastic scattering $D_{\mathrm{inel}} = 10^{-1}$ eV^2 and $\hbar\omega_{\mathrm{inel}} = 25$ meV.

barrier height this problem is less apparent, since even at low drain voltages electrons do not tunnel through the drain sided-barrier.

It should be noticed that, as opposed to conventional MOSFETs, increasing the length of the ungated area, L_{DG}, does not increase the resistance. In conventional MOSFETs the intrinsic resistivity of the channel is high. The resistivity of the channel is modulated, when the gate voltage attracts or repels carriers from the channel. As a result the resistance of the ungated region is high. In CNTs the intrinsic conductance is fixed and independent from the gate voltage.

In conventional MOSFETs carrier transport is diffusive, while in CNT based transistors carrier transport is nearly ballistic. To make a fair comparison with conventional MOSFETs, the effect of L_{DG} on the output characteristics is investigated for both ballistic and diffusive transport limit. To study diffusive transport in CNT based transistors an artificially large value for the electron-phonon coupling constant and a small value for the phonon energy is chosen. Fig. 6 shows that even in the case of diffusive transport (similar to conventional MOSFETs) the ungated regime does not increase the resistance.

Conclusion

Experimental and theoretical predictions indicate that in CNTs either the electron-phonon coupling is weak or the phonon energy is high. It has been shown in this work that, as a consequence, CNT based devices can operate close to the ballistic limit. Furthermore, an appropriate selection of L_{SG} and L_{DG} improves the device performance considerably, and in contrast to conventional MOSFETs, the ungated region does not increase the channel resistance.

Acknowledgment

This work has been supported by the Austrian Science Fund, contract I79-N16, and and the national program for tera-level nano-devices of the Korean ministry of science and technology.

References

[1] A. Javey, J. Guo, Q. Wang, M. Lundstrom, and H. Dai, "Ballistic Carbon Nanotube Field-Effect Transistors," *Letters to Nature*, vol. 424, no. 6949, pp. 654–657, 2003.

[2] J. Appenzeller, M. Radosavljevic, J. Knoch, and P. Avouris, "Tunneling Versus Thermionic Emission in One-Dimensional Semiconductors," *Phys.Rev.Lett.*, vol. 92, p. 048301, 2004.

[3] M. Pourfath, A. Gehring, E. Ungersboeck, H. Kosina, S. Selberherr, B.-H. Cheong, and W. Park, "Separated Carrier Injection Control in Carbon Nanotube Field-Effect Transistors," *J.Appl.Phys.*, vol. 97, pp. 1 061 031–1 061 033, 2005.

[4] M. Pourfath, E. Ungersboeck, A. Gehring, W. J. Park, B. H. Cheong, H. Kosina, and S. Selberherr, "Optimization of Schottky Barrier Carbon Nanotube Field Effect Transistors," *Microelectronic Engineering*, vol. 81, no. 2-4, pp. 428–433, 2005.

[5] G. Mahan, "Electron-Optical Phonon Interaction in Carbon Nanotubes," *Phys.Rev.B*, vol. 68, p. 125409, 2003.

[6] J. Park, S. Rosenblatt, Y. Yaish, V. Sazonova, H. Ustunel, S. Braig, T. Arias, P. Brouwer, and P. McEuen, "Electron-Phonon Scattering in Metallic Single-Walled Carbon Nanotubes," *Nano Lett.*, vol. 4, no. 3, pp. 517–520, 2004.

[7] M. Pourfath, H. Kosina, and S. Selberherr, "Rigorous Modeling of Carbon Nanotube Transistors," *IOP J.Phys.:Conf.Ser.*, vol. 38, pp. 29–32, 2006.

[8] A. Svizhenko and M. Anantram, "Effect of Scattering and Contacts on Current and Electrostatics in Carbon Nanotubes," *Phys.Rev.B*, vol. 72, pp. 085 430–085 440, 2005.

[9] J. Guo, "A Quantum-Mechanical Treatment of Phonon Scattering in Carbon Nanotube Transistors," *J.Appl.Phys.*, vol. 98, p. 063519, 2005.

[10] A. Javey, J. Guo, D. Farmer, Q. Wang, E. Yenilmez, R. Gordon, M. Lundstrom, and H. Dai, "Self-Aligned Ballistic Molecular Transistors and Electrically Parallel Nanotube Arrays," *Nano Lett.*, vol. 4, no. 7, pp. 1319–1322, 2004.

[11] M. Radosavljevic, S. Heinze, J. Tersoff, and P. Avouris, "Drain Voltage Scaling in Carbon Nanotube Transistors," *Appl.Phys.Lett.*, vol. 83, no. 12, pp. 2435–2437, 2003.